Quantum Electronics **49** (3) 293–297 (2019)

https://doi.org/10.1070/QEL16883

Impact of microwave-field inhomogeneity in an alkali vapour cell using Ramsey double-resonance spectroscopy

W. Moreno, M. Pellaton, C. Affolderbach, N. Almat, M. Gharavipour, F. Gruet, G. Mileti

Abstract. **We numerically and experimentally evaluate the impact of the inhomogeneity of the microwave field in the cavity used to perform double-resonance (DR) Ramsey spectroscopy in a buffer gas alkali vapour cell. The Ramsey spectrum is numerically simulated using a simple theoretical model and taking into account the field distribution in a magnetron-type microwave resonator. An experimental evaluation is performed using a DR pulsed optically pumped (POP) atomic clock. It is shown that the sensitivity to the microwave power of the DR POP clock can be reproduced from the combination of two inhomogeneities across the vapour cell: microwave field inhomogeneity and atomic ground-state resonance frequency inhomogeneity. Finally, we present the existence of an optimum operation point for which the microwave power sensitivity of our DR POP clock is reduced by two orders of magnitude. It leads into a long-term frequency stability of 1×10^{-14}.**

Keywords: *microwave-power frequency shift, microwave field amplitude inhomogeneity, double-resonance clock, POP clock, rubidium, magnetron-type cavity, vapour cell.*

1. Introduction

Vapour-cell frequency standards combine reduced volume and power consumption while maintaining excellent frequency stability performances. Among the laboratory prototype clocks are continuous-wave (cw) [1–3] or pulsed optically pumped (POP) [4–6] double-resonance (DR) clocks, or cw [7] or pulsed [8, 9] coherent population trapping (CPT) clocks. Compact cold caesium atomic clocks [10] are also currently in development. Most of the recent laboratory atomic clock prototypes demonstrate frequency stabilities at $\tau = 1$ s in the range of $(2–6)\times10^{-13}\tau^{-1/2}$ and reach in the medium-to-long terms the level of 10^{-14}, for integration times larger than $\tau > 10^4$ s. The main limiting factors on these time scales arise from the clock frequency sensitivities to instabilities in the atoms' environment: light source's intensity or frequency through the light shift effects, the microwave power, other environmental parameters such as residual static magnetic field, temperature, atmospheric pressure [11], and humidity. Ultimately, the long-term stability of the atomic clock is limited by aging processes.

In the case of rubidium (Rb) vapour-cell DR POP atomic clocks, the origin of the clock frequency sensitivity to the variations of the amplitude of the microwave field in the resonance cell was identified to result from two distinct mechanisms. The first mechanism is due to the cavity pulling effect which is related to the frequency mismatch between the rubidium ground state splitting frequency and the microwave-cavity resonance frequency [12]. The second mechanism is the position-shift effect. The resonance frequency of a group of Rb atoms will be different from another group of atoms in the vapour cell because of inhomogeneous electric, magnetic and electro-magnetic (EM) fields. The measured clock frequency is a weighted average of the resonance frequencies of each group of atom. Any change in the microwave power will modify the weighting inside the vapour cell which results in a clock frequency change [13, 14]. Note that this description is valid only for buffer gas cells in which the change of position of each atom during a Ramsey cycle may be considered as negligible.

In this work, we evaluate the impact of the microwave magnetic field amplitude inhomogeneity and its weighting of the atomic resonance frequencies distributed within the cell on the properties of the central Ramsey fringe with an emphasis on its (1) contrast, (2) full-width-at-half-maximum (FWHM), and (3) central fringe centre-frequency (CFCF) detuning obtained in a DR POP Rb clock experiment. We first review the basic theoretical model describing the DR POP scheme in the 3-level approximation. We decompose our vapour cell into a 3D mesh (of 1800 points) where each point of the mesh has different value of microwave magnetic field amplitude (based on the simulated microwave magnetic field amplitude distribution for the magnetron-type microwave cavity used in our Rb clock prototype) and a different atomic resonance frequency. We evaluate the impact of the microwave magnetic field amplitude inhomogeneity by measuring the mentioned characteristics of the Ramsey central fringe in our DR POP clock prototype for various microwave powers. Finally, the results are discussed and we demonstrate that the microwave-power sensitivity of our DR POP atomic clock can be reproduced from the presence of microwave magnetic field amplitude inhomogeneity and atomic ground-state resonance frequency distribution across the cell.

2. Theoretical model

In this section, the double-resonance interaction (Fig. 1a) in the 3-level approximation of the ^{87}Rb D_2 line (Fig. 1c) is described according to the theory presented in [12, 15].

W. Moreno, M. Pellaton, C. Affolderbach, N. Almat, M. Gharavipour, F. Gruet, G. Mileti Laboratoire Temps-Fréquence, Institut de Physique, Université de Neuchâtel, Avenue de Bellevaux 51, 2000 Neuchâtel, Switzerland; e-mail: william.moreno@unine.ch; gaetano.mileti@unine.ch

Received 24 October 2018; revision received 11 December 2018
Kvantovaya Elektronika **49** (3) 293–297 (2019)
Submitted in English

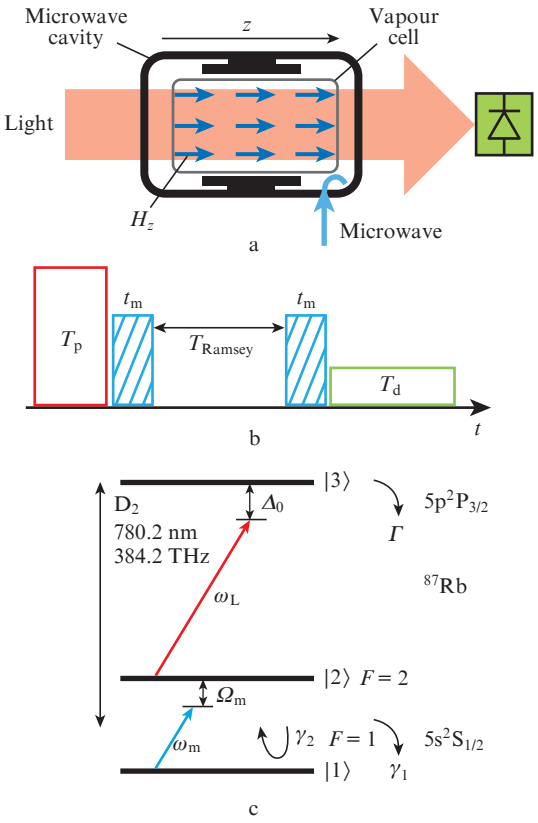

Figure 1. (a) Double-resonance interaction scheme, (b) POP timing scheme, and (c) three-level approximation of the ^{87}Rb D_2 line. Here, H_z is magnetic field strength of the microwave signal; ω_L and ω_m are the optical and microwave frequencies; $\Delta_0^i = \omega_{3i} - \omega_L$ is the laser frequency detuning (i = 1, 2 are the numbers of the components of the ground state); $\Omega_m = \omega_{21} - \omega_m$ is the microwave frequency detuning; Γ is the excited state linewidth; γ_1 and γ_2 are the ground state population and coherence relaxation rates, respectively; T_p, t_m, and T_d are the duration of the laser optical pump, microwave, and optical detection pulses, respectively; and T_{Ramsey} is the Ramsey delay.

The DR POP scheme theory can be understood physically using Bloch's vector representation. The atomic population is optically pumped into one of the ground state (Fig. 1b). As demonstrated in [12, 15], the state of the atomic population, at the end of the Ramsey scheme, can be expressed as the matrix product (in the rotating wave approximation):

$$R(t_{end}) = M_m(t_m)M_D(T_{Ramsey})M_m(t_m)R(0), \quad (1)$$

where $t_{end} = T_{Ramsey} + 2t_m$ is the duration of the Ramsey scheme and $t = 0$ corresponds to the end of optical pumping. The matrix M_m describes the microwave interaction and is given by [12, 15]:

$$M_m(t) = \begin{pmatrix} \cos(\xi t) & \frac{\Omega_m}{\xi}\sin(\xi t) & -\frac{b}{\xi}\sin(\xi t) \\ -\frac{\Omega_m}{\xi}\sin(\xi t) & \frac{b^2+\Omega_m^2\cos(\xi t)}{\xi^2} & \frac{\Omega_m b}{\xi^2}(1-\cos(\xi t)) \\ \frac{b}{\xi}\sin(\xi t) & \frac{\Omega_m b}{\xi^2}(1-\cos(\xi t)) & \frac{\Omega_m^2+b^2\cos(\xi t)}{\xi^2} \end{pmatrix}. \quad (2)$$

Here, $\xi^2 = \Omega_m^2 + b^2$, where b is the microwave Rabi frequency. In the case of zero microwave detuning, the matrix M_m is reduced to a rotation matrix around the y axis by an angle $\theta = bt_m$, which is usually called the microwave pulse area and represents the rotation angle of the Bloch vector during one microwave pulse in the Bloch sphere representation. The matrix M_D describes the free evolution of the Bloch vector $R(t)$ and is given by [12, 15]:

$$M_D(t) = \begin{pmatrix} \exp(-\gamma_2 t)\cos(\Omega_m t) & \exp(-\gamma_2 t)\sin(\Omega_m t) & 0 \\ -\exp(-\gamma_2 t)\sin(\Omega_m t) & \exp(-\gamma_2 t)\cos(\Omega_m t) & 0 \\ 0 & 0 & \exp(-\gamma_1 t) \end{pmatrix}, \quad (3)$$

$$R(t) = \begin{pmatrix} 2\,\mathrm{Re}(\delta_{12}(t)) \\ 2\,\mathrm{Im}(\delta_{12}(t)) \\ \Delta(t) \end{pmatrix}, \quad (4)$$

where δ_{12} is the ground state coherence; $\Delta = \rho_{22} - \rho_{11}$; and ρ_{ii} is the density of atoms in one of the ground state levels $|i\rangle$. The Ramsey spectrum is obtained by computing $R_3(t_{end}) = \Delta(t_{end})$ as a function of the microwave frequency detuning Ω_m. The cell volume is decomposed into a mesh with the division sizes given below.

Size of the absorption cell	
diameter/mm	25
length/mm	25
Size of the subdivisions	
Δ_x/mm	2
Δ_y/mm	2
Δ_z/mm	1
Optical absorption cross section	
σ_{13}/m^2	1.3×10^{-15}
σ_{23}/m^2	1.6×10^{-15}
n_0/m^{-3}	2.89×10^{17}
Theoretical D_2 linewidth of the optical transition,	
Γ/GHz	2.5
Population and coherence relaxation rates	
γ_1/Hz	360
γ_2/Hz	340

A certain value of the microwave magnetic field amplitude is associated to each point of the mesh and the Ramsey spectra are computed using the matrix product (1) at each point assuming a perfect optical pumping. With the Beer–Lambert law applied for the optical detection pulse (see Fig. 1b), the intensity at the end of the vapour cell is given by:

$$I_i(L_{cell}) = I(0)\exp\left(-\sigma_{i3}n_0\sum_j \rho_{ii}(z_j)\Delta z\right), \quad (5)$$

where $I(0)$ is the detection light intensity at the entrance of the vapour cell; σ_{i3} is the optical absorption cross section for the transition $|i\rangle \rightarrow |3\rangle$; $\rho_{ii}(z_j)$ is the density of atoms in one of the ground state levels at the point z_j; and Δz is the z-axis integration step.

3. Experimental setup

The numerical simulations are compared with the Ramsey spectra measured using our POP DR Rb atomic clock prototype. Details of the clock were previously presented in [3, 5]. Our clock prototype is based on a home-made ^{87}Rb-enriched vapour glass cell, 25-mm long and 25 mm in diameter, with a

buffer gas mixture of argon and nitrogen ($P_{Ar}/P_{N_2} = 1.6$). The laser used for both optical pumping and detection pulses is frequency stabilised to one of the sub-Doppler transition frequencies, $|^2S_{1/2}, F = 1\rangle \rightarrow |^2P_{3/2}, F' = 0/F' = 1\rangle$ or $|^2S_{1/2}, F = 2\rangle \rightarrow |^2P_{3/2}, F' = 3\rangle$, of the ^{87}Rb D_2 line. The microwave cavity is a magnetron-type cavity [16] with a loaded quality factor of $Q_L = 185$. The microwave magnetic field amplitude distribution is shown in Fig. 2. The clock setup is operated in the POP DR scheme [4] where the duration of each pulse is set as follows: $T_p = 0.4$ ms, $t_m = 0.3$ ms, $T_{Ramsey} = 3$ ms, and $T_d = 0.7$ ms.

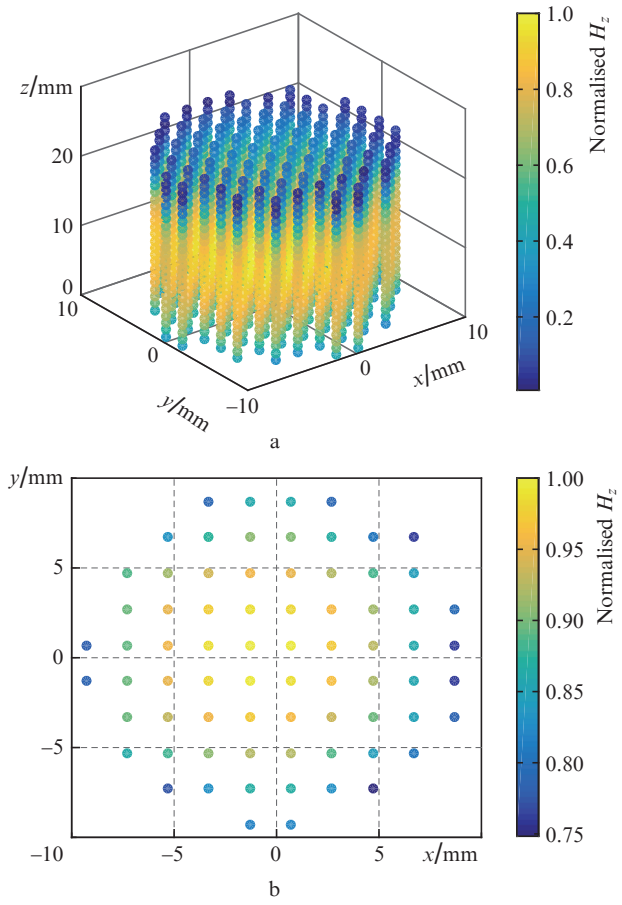

Figure 2. (a) Simulated microwave magnetic field distribution inside the vapour cell performed at the Laboratory of Electromagnetics and Acoustics (LEMA-EPFL) and (b) transverse distribution of the magnetic field at $z = 9$ mm.

4. Results

In this section, the Ramsey spectrum is obtained in three cases: numerical simulation with homogeneous microwave magnetic field amplitude distribution, numerical simulation with inhomogeneous microwave magnetic field amplitude distribution, and measurement using our POP Rb clock. These Ramsey spectra are obtained for different values of the microwave pulse area $\theta = bt_m$ with $b \propto \sqrt{P_m}$ and for a fixed t_m. Here, P_m is the microwave power. For each spectrum, we are interested in its contrast, full-width-at-half-maximum, and CFCF detuning.

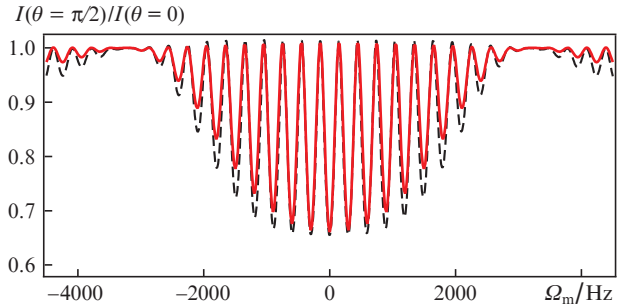

Figure 3. Simulated (solid curve) and measured (dashed curve) Ramsey spectra.

4.1. Ramsey spectrum

Figure 3 presents the calculated light intensity at the end of the vapour cell $I(\theta = \pi/2)$ as a function of the microwave frequency detuning Ω_m and the measured Ramsey spectrum. The light intensity is obtained according to equation (5) after one cycle of microwave interrogation described by equation (1) in the case of $\pi/2$ microwave pulses considering the microwave magnetic field amplitude distribution of Fig. 2 with the experimental conditions listed above. The Ramsey spectra are normalised to the light intensity detected at the end of the vapour cell in the absence of any microwave interrogation (i.e. $P_m = 0$). In the low microwave detuning region, we obtain a good agreement between the Ramsey spectrum measured using our POP Rb atomic clock and the computed one.

4.2. Central fringe contrast

The variation of the contrast of the central Ramsey fringe in Fig. 4 as a function of the microwave power corresponds to the population oscillations in the ground state. It is equivalent to the Rabi oscillations where the ground state population varies with the combined microwave pulse area 2θ. Experimentally, we detect the change in the transmitted light at zero microwave frequency detuning as a function of the microwave power. The contrast of the central fringe is defined as the relative change in the optical absorption [5]:

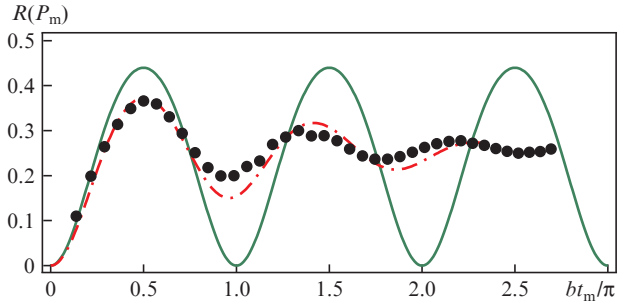

Figure 4. Rabi oscillations simulated for (solid curve) homogeneous and (dashed curve) inhomogeneous microwave field and (points) measured Rabi oscillations (Ramsey spectrum central fringe contrast) at $\Omega_m = 0$. The horizontal axis is normalised such that the first maximum occurs for two $\pi/2$ microwave pulses (i.e. $\theta = bt_m = \pi/2$).

$$R = 1 - \frac{I(P_m, \Omega_m = 0)}{I(0, \Omega_m = 0)}. \quad (6)$$

The quantity R obtained numerically as well as experimentally is shown in Fig. 4. The results are consistent with the Rabi oscillations measured using our POP Rb atomic clock and with previously reported observations [5].

4.3. Central fringe FWHM

Figure 5 presents the FWHM of the central Ramsey fringe as a function of bt_m. The central Ramsey fringe is obtained via measurement and simulation in the cases of homogeneous and inhomogeneous microwave field amplitude distributions. Let ω_H be the half width at half maximum (HWHM) of the central fringe ($\omega_F = 2\omega_H$). Figure 5 presents the values of ω_F determined from the ω_H solution of the equation:

$$T_{Ramsey}\omega_H + 2\phi_0(b, \omega_H) = \pi/2, \quad (7)$$

where

$$\phi_0(b, \omega_H) = \arctan\left(\frac{\omega_H}{\sqrt{b^2 + \omega_H^2}} \frac{1 - \cos(\xi t_m)}{\sin(\xi t_m)}\right). \quad (8)$$

A good agreement between the inhomogeneous microwave magnetic amplitude distribution case and the measurement is obtained. Moreover, we obtain a good agreement between the homogeneous microwave magnetic amplitude case and ω_H solution of equation (7).

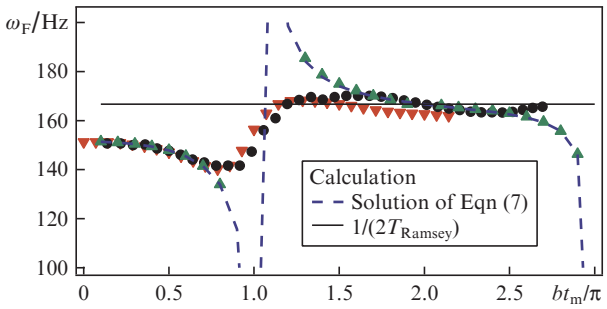

Figure 5. Simulated FWHM of the Ramsey spectrum central fringe for (▲) homogeneous and (▼) inhomogeneous microwave field distributions, and (●) results of experimental measurements.

4.4. Central fringe frequency shift

Figure 6a presents the measured microwave-power sensitivity of our DR POP clock. The frequency of the central fringe of the Ramsey spectra simulated as a function of bt_m is shown in Fig. 6b. The numerical calculation was performed taking into account not only the microwave magnetic amplitude distribution of Fig. 2 but also a ground-state frequency shift $\Delta f(\boldsymbol{r}, t)$ distribution among the vapour cell. Two cases are considered: homogeneous frequency shift distribution [$\Delta f(\boldsymbol{r}, t) =$ 1 Hz] and inhomogeneous frequency shift distribution. In order to reproduce the experimental data, at each point of the mesh, we assumed the following empirical frequency shift distribution that mimics a residual coherence at the end of the optical pump pulse [12]:

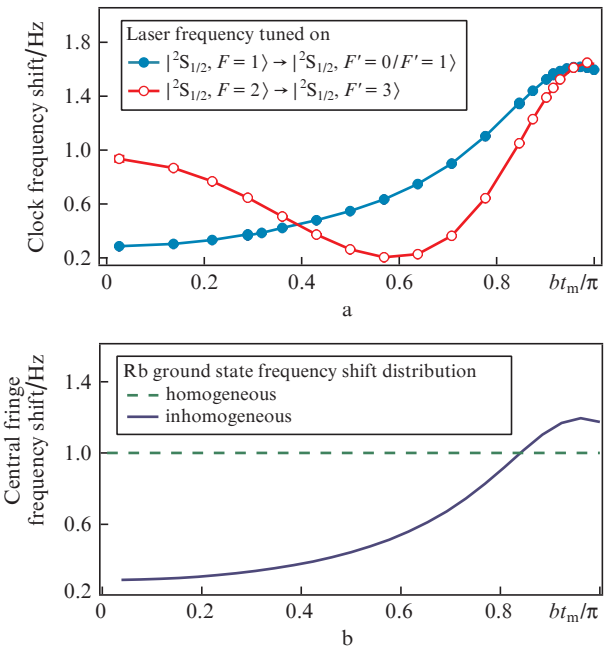

Figure 6. (a) Measured microwave power sensitivity of the clock frequency and (b) simulated microwave power sensitivity of the central fringe frequency. Frequency shifts are presented with respect to the frequency of 6.8346868658 GHz.

$$\Delta f(\boldsymbol{r}, t) = C\exp\left(-\left(\gamma_2 + \frac{\Gamma_{op}(\boldsymbol{r}, t)}{\delta_0^2 + 1}\right)T_p\right)\sin\left(\frac{\Gamma_{op}(\boldsymbol{r}, t)\delta_0}{\delta_0^2 + 1}T_p\right), \quad (9)$$

where C is an empirical constant; $\Gamma_{op}(\boldsymbol{r}, t)$ is the optical pumping rate; and $\delta_0 = 2\Delta_0/\Gamma$. The analysis of the physical origins of this inhomogeneous shift will constitute the subject of a separate study. Two of the main candidate effects are however already identified: the AC Stark shift and the residual coherence after optical pumping pulse.

5. Analysis and discussion

In the case of a homogeneous microwave magnetic field amplitude distribution, all the atoms in the vapour cell undergo the same microwave pulse. All the groups of atoms produce the same Ramsey spectrum and are identical to the output Ramsey spectrum. Its contrast is maximal for the ($\pi/2$ + $n\pi$) pulse and is zero for (π + $n\pi$) pulse. For a π pulse, no fringes are observed and the FWHM cannot be defined, which explains the discontinuity of the $\omega_F(bt_m)$ dependence at bt_m = π in Fig. 5.

For an inhomogeneous microwave magnetic field amplitude distribution, different groups of atoms in the vapour cell undergo slightly different microwave pulses. It results that the output Ramsey spectrum is an average of each Ramsey spectrum generated inside the cell. The consequence is that a residual central fringe at $bt_m = (\pi + n\pi)$ is in this case present. Thus a non-zero contrast (Fig. 4) and the ω_F (Fig. 5) can be determined for $bt_m = (\pi + n\pi)$.

The microwave-power sensitivity of the CFCF is reproduced as consequence of two inhomogeneities: rubidium ground-state resonance frequency shift distribution and micro-

wave magnetic field amplitude distribution. The output Ramsey spectrum is an average of the Ramsey spectra generated from each group of atoms in the vapour cell. Each group of atoms has a contribution that depends on the microwave pulses that they undergo. However, for a homogeneous resonance frequency shift distribution each group of atoms contributes with a different weight but with the same frequency shift (e.g. no shift is induced by the microwave coupling), which explains the absence of microwave-power sensitivity of the CFCF. In the case of an inhomogeneous resonance-frequency shift distribution, the inhomogeneous microwave field weights these various local shifts. When changing the microwave power ($\theta = bt_m \propto \sqrt{P_m}\, t_m$) the weight distribution changes which gives rise to the microwave-power sensitivity of the CFCF in Fig. 6.

Finally, the experimental data of Fig. 6a shows that an operation point exists to reduce the microwave-power sensitivity coefficient in our POP DR clock. This occurs when the laser frequency is tuned on the $|^2S_{1/2}, F = 2\rangle \rightarrow |^2P_{3/2}, F' = 3\rangle$ transition and for a microwave pulse with $bt_m = 0.57\pi$. In this condition, we measured a microwave-power sensitivity coefficient at the level of $4.5\times10^{-14}\ \mu W^{-1}$ which is two orders of magnitude lower than the previously reported coefficient [17]. Operating our DR POP clock in these conditions, we have reported a long-term relative frequency stability of 1×10^{-14} [18].

In conclusion, we have analysed the impact of the microwave magnetic field amplitude inhomogeneity on Ramsey spectroscopy. Based on a theoretical model describing the Ramsey spectroscopy, we demonstrated the impact of the microwave field amplitude inhomogeneity and the resonance-frequency distribution on the Ramsey spectrum, in particular on the contrast, the FHWM, and the frequency detuning of the central fringe. We obtained excellent agreement between the numerical simulation and the measurement in each case. Especially, we demonstrated that the microwave-power sensitivity of our POP DR atomic clock can be reproduced from the presence of two inhomogeneities: microwave-power inhomogeneity and atomic resonance frequency inhomogeneity. Further studies are necessary in order to study and ideally suppress the latter.

Acknowledgements. This work was supported by the Swiss National Science Foundation (SNSF Grant No. 156621). The authors thank M. Dürrenberger and P. Scherler (both LTF, University of Neuchâtel, Switzerland) for technical support. We also thank A. Skrivervik and A.E. Ivanov (EPFL-MAG, Switzerland) for fruitful collaborations on microwave cavity developments and simulations.

References

1. Mei G., Zhong D., An S., Zhao F., Qi F., Wang F., Ming G., Li W., Wang P., in *Proc. 2016 European Frequency and Time Forum (EFTF)* (York, 2016) p. 275.
2. Hao Q., Li W., He S., Lv J., Wang P., Mei G. *Rev. Sci. Instrum.*, **87**, 123111 (2016).
3. Bandi T., Affolderbach C., Stefanucci C., Merli F., Skrivervik A.K., Mileti G. *IEEE Trans. Ultrason., Ferr., Freq. Control*, **61** (111), 1769 (2014).
4. Micalizio S., Calosso C.E., Godone A., Levi F. *Metrologia*, **49**, 425 (2012).
5. Kang S., Gharavipour M., Affolderbach C., Gruet F., Mileti G. *J. Appl. Phys.*, **117**, 104510 (2015).
6. Dong G., Deng J., Lin J., Zhang S., Lin H., Wang Y. *Chin. Opt. Lett.*, **15**, 040201 (2017).
7. Cyr N., Tetu M., Breton M. *IEEE Trans. Instr. Meas.*, **42**, 640 (1993).
8. Abdel Hafiz M., Coget G., Petersen M., Calosso C.E., Guérandel S., de Clercq E., Boudot R. *Appl. Phys. Lett.*, **112**, 244102 (2018).
9. Yun P., Tricot F., Calosso C.E., Micalizio S., Francois B., Boudot R., Guerandel S., de Clercq E. *Phys. Rev. Appl.*, **7** (11), 014018 (2017).
10. Esnault F.-X., Blanshan E., Ivanov E.N., Scholten R.E., Kitching J., Donley E.A. *Phys. Rev. A*, **88** (14), 042120 (2013).
11. Moreno W., Pellaton M., Affolderbach C., Mileti G. *IEEE Trans. Ultrason., Ferr., Freq. Control*, **65** (8), 1500 (2018).
12. Godone A., Micalizio S., Levi F. *Phys. Rev. A*, **70** (12), 023409 (2004).
13. Risley A., Busca G., in *32nd Annual Symposium on Frequency Control* (Atlantic City, NJ, USA, 1978) p. 506.
14. Micalizio S., Godone A., Levi F., Calosso C. *Phys. Rev. A*, **79** (11), 013403 (2009).
15. Vanier J., Audoin C. *The Quantum Physics of Atomic Frequency Standards* (Philadelphia: Adam Hilger, 1989).
16. Stefanucci C., Bandi T., Merli F., Pellaton M., Affolderbach C., Mileti G., Skrivervik A.K. *Rev. Sci. Instrum.*, **83**, 104706 (2012).
17. Gharavipour M., Affolderbach C., Kang S., Bandi T., Gruet F., Pellaton M., Mileti G. *J. Phys. Conf. Ser.*, **723**, 012006 (2016).
18. Affolderbach C., Almat N., Gharavipour M., Gruet F., Moreno W., Pellaton M., Mileti G., in *IEEE International Frequency Control Symposium (IFCS)* (Olympic Valley, CA, USA, 2018) p. 1-6, DOI: 10.1109/FCS.2018.8597452.